https://doi.org/10.1016/j.engstruct.2021.112435

Behaviour and design of cold-formed austenitic stainless steel circular tubes infilled with seawater sea-sand concrete

Yancheng Cai [a], Albert K.H. Kwan [b,*]

[a] Department of Civil and Environmental Engineering, The Hong Kong Polytechnic University, Hong Kong, China (Formerly, Department of Civil Engineering, The University of Hong Kong, Pokfulam Road, Hong Kong, China)

[b] Department of Civil Engineering, The University of Hong Kong, Pokfulam Road, Hong Kong, China

Abstract: Infilling seawater sea-sand concrete (SWSSC) into stainless steel tubes may be a feasible means of overcoming the shortage of fresh water and river sand in remote coastal areas. Herein, cold-formed austenitic stainless steel (CFASS) circular tubular stub columns infilled with SWSSC were tested. The CFASS tubes had 5 different cross-sections and the concrete mixes were of strength levels 35 and 70 MPa. Axial compression tests were carried out to study their structural behaviour in terms of load-strain curve, strength, ductility and failure mode. The test results revealed that the use of SWSSC in place of conventional concrete in stainless steel tubes has little effect on the structural behaviour and thus should be feasible. The test results were also compared with predictions by existing design equations in the codes and literature. It was found that the existing design equations are either un-conservative or overly conservative. Based on the test results in this study and those in literature, a new and more accurate design equation for axially loaded concrete-filled stainless steel circular tubular stub columns that is applicable to different types of concrete infill, including conventional concrete and SWSSC, was proposed.

Keywords: Concrete-filled steel tubes; confinement effects; seawater sea-sand concrete; stainless steel structures; stub columns.

---

* Corresponding author.
E-mail address: khkwan@hku.hk (A.K.H. Kwan).

1. Introduction

Concrete-filled steel tubes (CFSTs) have become quite widely used in various structural members, such as columns in buildings and chord members in bridges, due to their excellent structural performance acquired from the synergistic actions of the steel tube providing confinement to the concrete core and the concrete core delaying or preventing local buckling of the steel tube [1,2]. Recently, their possible applications in submarine pipeline structures have also been explored [3,4]. In fact, CFSTs can be applied to all kinds of linear structural members subjected to axial compression. Among CFST columns, circular tubular ones are the most popularly used. They provide superior strength enhancement and ductility [5] as well as post-yield capacity [6] than those of square or rectangular tubular ones. In the last few decades, great efforts have been made to research the behaviour and design of circular tubular CFST columns, as summarized in the references [7-11]. With advancements in materials technology, higher performance materials have become available, for examples, steel tubes with proof stress higher than 1000 MPa [12] and concretes with cylinder strength up to 190 MPa [13]. These advancements have led to the development of high performance CFST columns made of high-strength steel and high-strength concrete [13].

On the other hand, for sustainable development, efforts are being made to develop more environmental-friendly construction. Due to the acute shortage of fresh water and river sand in many places, especially remote coastal areas [14,15] and the large carbon footprint of cement manufacturing, which has been causing global warming [16], it has been advocated in recent years to reduce fresh water, river sand and cement consumptions. To solve these problems, various attempts from the materials standpoint have been made, such as using seawater and sea-sand to replace fresh water and river sand [17-21], adding alkali activated binders to completely replace cement [22-26], and adding limestone fines [27-31] to partially replace cement etc. Attempts from the structural standpoint of employing more efficient structural forms, such as CFSTs, to make better use of concrete and reduce cement consumption have also been made, as in the present study.

The uses of seawater and sea-sand to replace fresh water and river sand have led to the development of seawater sea-sand concrete (SWSSC) and SWSSC structures [32-35]. Due to the corrosive condition caused by the chloride ions in the seawater and sea-sand, the conventional steel reinforcing bars and tubes are no longer suitable, and stainless steel or fibre reinforced polymer (FRP) bars and tubes will have to be employed [32]. As stainless steel and FRP are relatively new materials with different mechanical properties, more research is still needed to study their effects on the structural behaviour and develop design methods for their incorporation.

This research focuses on the combined usage of SWSSC and stainless steel tubes. It is proposed herein to infill SWSSC into stainless steel tubes to form CFSTs, which should have the advantages of reduced fresh water and river sand consumptions, and higher structural efficiency arising from the synergistic effects of the interaction between the internal concrete core and external steel tube. As there is little or no oxygen in the interior of the steel tube, the SWSSC would not cause corrosion of the inside surfaces of the steel tubes. Nevertheless, since such CFSTs are expected to be used in marine environment, which could cause corrosion of the outside surfaces of the steel tubes, it is still considered necessary to use the more corrosive resistant stainless steel tubes rather than the conventional steel tubes.

However, even the design of stainless steel tubular members infilled with conventional concrete has not yet been included in the existing codes [36-39], not to mention the design of stainless steel tubular members infilled with SWSSC. In this research, an attempt was made to investigate the structural behaviour and design of stainless steel circular tubular stub columns infilled with SWSSC and subjected to axial compression. The specimens tested were constructed of cold-formed austenitic stainless steel (CFASS) tubes and SWSSC of nominal cylinder strength 35 and 70 MPa. The test results were compared with predictions by the existing design methods in EC4 [36], AS5100 [37], AISC [38] and ACI [39], as well as those in the literature. Lastly, a new design equation for the axial strength of CFASS circular tubes infilled with different types of concrete, including SWSSC, was proposed.

2. Experimental investigation

2.1 Material properties of stainless steel tube

Grade AISI 304 (EN 1.4301) cold-formed austenitic stainless steel (CFASS) circular tubes were used as the outer skins for the stub column specimens. The nominal dimensions ($D \times t$) of the steel tubes were 60.5×2.8 mm, 76.3×3.0 mm, 114.3×3.0 mm, 139.4×3.0 mm and 165.2×3.0 mm. Curved coupons were machined from the circular tubes. Two sets of specially designed grips and pins were used to avoid load eccentricities in the curved coupon tests. They are the same as those detailed in Ma *et al*. [12]. The nominal gauge length and width of the curved coupons were 25 mm and 4 mm, respectively. On each coupon, two strain gauges were glued on both faces at mid-length and an extensometer was mounted. The coupons were tested in a 50-kN MTS testing machine under displacement control at loading rates of 0.05 mm/min and 0.5 mm/min within the elastic and plastic ranges, respectively. The Young's modulus (E_s) was determined from the strain gauges, while the other material properties were determined from the stress-strain curves obtained from the extensometer. The test results, including the E_s, 0.01% proof stress ($f_{0.01}$), 0.2% proof stress ($f_{0.2}$), ultimate strength (f_u), ultimate strain (ε_u) and fracture strain (ε_f), are presented in Table 1. The Ramberg-Osgood parameter n for describing the initial nonlinear part of the axial stress-strain curve, was obtained from the measured $f_{0.01}$ and $f_{0.2}$ proof stress values using the equation $n = ln(0.01/0.2)/ln(f_{0.01}/f_{0.2})$.

2.2 Seawater sea-sand concrete mixes

Two concrete strength levels, with target mean cylinder strengths (f_c) of 35 and 70 MPa, were adopted in this study. These strength levels were labelled as C35 and C70, and concrete mixes with such strength levels were designed following those of conventional concrete mixes with the same strength levels, as depicted in Table 2. The water/cement ratios of the concrete mixes with strength levels of C35 and C70 were 0.56 and 0.32, respectively. The fine aggregate had a maximum size of 5 mm, whereas the coarse aggregate had a maximum size of 10 mm. The ratio of fine aggregate to total aggregate in the concrete mix is set as 0.4. For each concrete strength level, one conventional concrete mix made with fresh water and ordinary fine aggregate, one seawater concrete mix made with seawater (in place of fresh water) and ordinary fine aggregate, and one seawater sea-sand concrete mix made with seawater (in place of fresh water) and sea-sand (in place of ordinary fine aggregate) were produced for testing. The ordinary fine aggregate and the coarse aggregate were both crushed granite rock with a solid density of 2610 kg/m^3. They were obtained from a quarry through a local supplier, whereas the sea-sand was obtained from the seabed through another local supplier. For easy reference, the conventional concrete mixes were labelled as

C35 or C70, according to their strength levels, while the seawater concrete mixes were labelled as SW-C35 or SW-C70, and the seawater sea-sand concrete mixes were labelled as SW-SS-C35 or SW-SS-C70 (note: SW stands for seawater and SS stands for sea-sand).

The seawater used was obtained from the seaside near the University of Hong Kong in Hong Kong. Its chemical compositions were measured as follows. The cations of the seawater were measured by Inductively Coupled Plasma - Optical Emission Spectroscopy using the equipment model Agilent 5110. Three introductions were conducted and the average results are shown in Table 3, where the compositions of Na^{+}, Mg^{2+}, K^{+} and Ca^{2+} are 1.04%, 0.14%, 0.06% and 0.05%, respectively. The anions of the seawater were measured by High Performance Liquid Chromatography with Conductivity Detector using the equipment model Shimadzu CDD-10Avp. Three injections were conducted and the average results are shown in Table 3, where the compositions of Cl^{-} and SO_4^{2-} are 2.55% and 0.24%, respectively.

The six concrete mixes, namely, C35, C70, SW-C35, SW-C70, SW-SS-C35 and SW-SS-C70, had been tested for their workability and strength in terms of slump and 28-day cylinder strength, respectively, as presented in Table 4. The slump test was carried out using a standard slump cone whereas the cylinder strength test was carried out by casting 150 mm diameter × 300 mm height cylinders for testing in accordance with the relevant European Standards. From each concrete mix, two cylinders were cast for testing at the age of 28 days, and another two cylinders were cast for testing at the time of testing the stub column specimens (about 2 months after casting). The average strength of the two cylinders tested at same time was taken as the concrete strength f_c. These results revealed that the use of seawater in place of fresh water had little effect on the workability and 28-day strength, while the use of sea-sand in place of ordinary fine aggregate had slightly increased the workability at both strength levels of C35 and C70, but slightly decreased the 28-day strength at strength level of C35 and slightly increased the 28-day strength at strength level of C70. The slight increase in workability was probably because of the more rounded shape of the sea-sand particles. Overall, it may be said that the uses of seawater and sea-sand have little effects on the workability and 28-day strength of the concrete produced.

2.3 Stub column specimen design and labelling

As explained before, the CFASS tubes have 5 different cross sections. For reflecting the effects of the infilled concrete, the unfilled CFASS circular stub columns i.e., the unfilled CFASS tubes, were tested first, as depicted in Table 5. The specimens were labelled according to their nominal ($D \times t$) dimensions, as listed in the first column of the table. However, the actual measured D and t dimensions were slightly different, as reported in the second and third columns of the table. The length (L) of each CFASS tube was set as $2.5D$ in order to avoid overall buckling, as reported in the fourth column of the table. All the CFASS tubes were wire cut at both ends.

The 5 different sectional types of CFASS tubes were then each infilled with SW-C35, SW-C70, SW-SS-C35 or SW-SS-C70 to form 20 concrete infilled CFASS circular stub column specimens for testing, as depicted in Table 6. Each specimen was identified by a label starting with the steel tube label in the form of the nominal ($D \times t$) dimensions and following by the concrete label of SW-C35, SW-C70, SW-SS-C35 or SW-SS-C70. In addition to these 20 specimens, 6 repeated specimens, each marked with "-r" at the end of the specimen label, were also made for testing. In total, 26 concrete infilled CFASS circular stub column specimens were tested.

2.4 Test rig and operation

Figure 1 illustrates a typical test setup for the Specimen 165.2×3.0-SW-SS-C35. A 5000 kN capacity servo-controlled hydraulic testing machine was used to apply axial compressive force to the stub column specimen. Four 50 mm range LVDTs were used to measure the end shortening of the specimen. These four LVDTs were placed between the top and bottom bearing plates at evenly spaced positions. To prevent "elephant foot" failure, end stiffeners in the form of steel rings with 30 mm width were screwed onto the specimen near its ends prior to testing. As the top surface of the infilled concrete might not be at the same level as the end of the steel tube due to shrinkage of the concrete, a high-strength plaster material was used to fill the small gap between the steel tube and the infilled concrete [40].

A ball bearing was placed at the top end of the specimen. An initial pre-load of 5 kN was applied before testing in order to close any gaps between the specimen and the contact surfaces of the testing machine. The compressive load was applied under displacement control at a constant rate of 0.5 mm/min until the load had reached a peak value and then dropped by more than 15%. Due to limited stroke of the actuator of the testing machine, the test was sometimes stopped earlier just after the axial shortening of the specimen had reached 15 mm. A data logger was used to record the readings from the LVDTs and the testing machine at time intervals of 1 second. Photographs were taken during the test to record the failure model.

3. Test results

3.1 Load-strain curves

The applied load versus axial strain curve of each column specimen, in which the applied load was taken from the testing machine and the axial strain was calculated as the average of the four LVDT readings divided by the specimen length (L), is plotted in Figures 2-6 for the specimens with steel tube ($D \times t$) sizes of 60.5×2.8, 76.3×3.0, 114.3×3.0, 139.4×3.0 and 165.2×3.0, respectively. From the curves plotted, it is evident that the strength of each CFASS circular stub column was substantially enhanced by the infilled concrete, indicating that the SWSSC infilled into the CFASS tubes was very effective in strengthening the CFASS tubes.

From the load-strain curves, the first peak load within 2% axial strain (P_{peak}), the proof load at 2% axial strain ($P_{2\%}$) and the ultimate load (P_u) are obtained, as tabulated in Tables 5 and 6. It should be noted that sometimes, there was no peak in the load-strain curve within 2% axial strain and the value of P_{peak} in such case is just given as "-". Moreover, since the test had to be stopped when the axial shortening of the specimen exceeded 15 mm albeit the load was still increasing and had not reached the ultimate yet, the value of P_u in such case is just taken as the maximum load recorded during the test, as marked by an asterisk "*" in the table. For detailed analysis and design, the yield load (P_y) is taken herein as the first peak load within 2% axial strain (P_{peak}) or the proof load at 2% axial strain ($P_{2\%}$), whichever is the larger, as in the case of conventional concrete filled steel tubular columns [41,42].

The load-strain curves of the repeated specimens (with "-r" marked at the end of the specimen label) are compared with those of the respective original specimens in Figure 7. Likewise, the P_{peak}, $P_{2\%}$ and P_u values of the repeated specimens have also been tabulated in Table 6 for comparison. From these comparisons, it can be seen that the load-strain curves and the P_{peak}, $P_{2\%}$ and P_u values of the repeated specimens agree quite well with those of the respective original specimens, indicating that the tests conducted were repeatable and thus reliable.

3.2 Overall axial performance

The load-strain curves of the CFASS tubes infilled with SW-C35, SW-C70, SW-SS-C35 or SW-SS-C70 are on the whole very similar to those of the same CFASS tubes infilled with conventional concrete of similar strength level [43]. This reveals that the uses of seawater and sea-sand in place of fresh water and ordinary fine aggregate in the concrete infill have no major effects on the axial behaviour. In other words, the use of SWSSC in place of conventional concrete as concrete infill in CFASS tubes also provides sound axial performance.

Comparing the specimens infilled with concretes of the same strength level, it is seen that the CFASS tubes infilled with SW-SS-C35 generally have yield load (P_y) about 5% to 10% lower than the respective CFASS tubes infilled with SW-C35, whereas the CFASS tubes infilled with SW-SS-C70 generally have yield load (P_y) about 5% lower to 5% higher than the respective CFASS tubes infilled with SW-C70. However, since at the time of testing, the concrete SW-SS-C35 had about 12% lower strength than the concrete SW-C35, and the concrete SW-SS-C70 had about 4% lower strength than the concrete SW-C70, it seems that the lower yield load of the CFASS tubes infilled with SW-SS-C35 or SW-SS-C70 was due to the lower strengths of the concrete infill. Anyway, since the decreases in yield load were rather small, it may be said that the use of sea-sand in place of ordinary fine aggregate in the concrete infill has little effect on the axial performance of the infilled CFASS tubes.

As for typical CFSTs with conventional concrete used as the infill, some of the specimens tested exhibited substantial strain-hardening responses, thereby imparting very high ductility to the axial behaviour of the CFASS tubes with SWSSC used as the infill. The substantial increases in ductility under axial compression may be attributed to the confinement effect of the external steel tube on the internal concrete core [43]. Apparently, the confinement effect was dependent on the relative sizes of the external steel tube and the internal concrete core, and the concrete strength level, as will be analysed in details in a later section.

3.3 Failure modes

For all the specimens not infilled with any concrete (i.e., all the hollow and unfilled CFASS tubes), both inward and outward local buckling occurred during testing, as depicted in the left sides of Figures 8-10, where the failure modes of some unfilled CFASS tubes are shown. Hence, the unfilled CFASS tubes failed not just by yielding, but also by local buckling. Nevertheless, for all the specimens infilled with concrete (i.e., all the infilled CFASS tubes), no inward buckling occurred due to restraint by the concrete core, and only minor outward bulging occurred at some locations, as depicted in the right sides of Figures 8-10, where the failure modes of some CFASS tubes infilled with SW-C70 are shown. Such restraint of the concrete core against local buckling of the CFASS tube had allowed the composite action between the steel tube and the concrete core to be more fully developed to exploit the synergistic effects of the steel tube confining the concrete core and the concrete core restraining local buckling of the steel tube.

In addition to the typical failure modes of CFASS tubes infilled with concrete made with seawater in place of fresh water depicted in Figures 8-10, the typical failure modes of CFASS tubes infilled with SWSSC are depicted in Figure 11. It is noted that the failure modes shown in Figure 11 are similar to those shown in Figures 8-10. Hence, the use of sea-sand in place of ordinary fine aggregate has little effect on the failure mode. One interesting point noted from these figures is that in the failure mode of each CFASS tube infilled with concrete, two obvious bulge-outs were formed at opposite faces at different heights indicating that the concrete core inside had an inclined shear crack formed due to shear sliding failure under tri-axial compression [42], as marked by a dashed line on the specimens in the figures. To illustrate the large shortening of the specimens associated with such bulge-outs, the length and shape of one typical specimen before testing and after testing are shown in Figure 12.

4. Detailed analysis of test results

4.1 Strength enhancement index

The synergistic effects of the composite action between the steel tube and the concrete core often increase the yield load (P_y) to substantially higher than the sum of the strength of the steel tube ($f_{0.2}A_s$) and the strength of the concrete core (f_cA_c), where A_s and A_c are the sectional areas of the steel tube and the concrete core, respectively. Such synergistic effects may be quantified in terms of the dimensionless strength enhancement index (*SEI*) defined by $SEI = P_y/(f_{0.2}A_s + f_cA_c)$. A *SEI* value of higher than 1.0 indicates positive enhancement of the yield load (P_y) due to the synergistic effects of the composite action. The *SEI* values of the specimens tested have been calculated, as presented in Table 7. From these *SEI* values, it can be seen that the *SEI* varies from 1.12 to 1.44 within range of structural parameters covered in this study.

To analyse how the *SEI* varied with the various structural parameters, the D/t ratio of the steel tube and the section constraining factor (ξ) defined by $\xi = f_{0.2}A_s/f_cA_c$ are also calculated, as listed in Table 7. Basically, the section constraining factor (ξ) is a measure of how strong the steel tube is relative to the concrete core. Together, the D/t ratio and the section constraining factor (ξ) govern the degree of confinement provided by the steel tube on the concrete core. To visualize the effects of these two parameters, the variation of the *SEI* with the D/t ratio is plotted in Figure 13 and the variation of the *SEI* with the value of ξ is plotted in Figure 14. It is seen that the *SEI* decreased as the D/t ratio increased, similar to the finding for high strength circular concrete filled steel tube short columns by Wei *et al*. [2]. On the other hand, the *SEI* increased as the value of ξ increased and then started decreasing when the value of ξ exceeded about 1.30. So, the highest *SEI* occurred when the value of ξ is around 1.30.

4.2 Infilled to unfilled strength factor

To evaluate the effectiveness of the concrete infill in increasing the strength of the tubular column, the ratio of the yield load of the CFASS tube infilled with concrete (listed in Table 6) to the respective yield load of the unfilled CFASS tube (listed in Table 5) has been worked out for each infilled CFASS tubular column specimen tested. Such infilled to unfilled strength ratio of the tubular column is hereafter abbreviated as the strength ratio, and the strength ratios so worked out are listed in the second last column of Table 7. It is evident from these strength ratios that the infilling of the CFASS tubes with SWSSC could increase the yield load to 4.80 times, or in other words, increase the yield load by up to 380%.

For graphical presentation, the variations of the strength ratio with the D/t ratio and the concrete strength are plotted in Figures 15(a) and 15(b). It should be noted that in Figure 15(b), the data points with concrete strength equal to zero are those of the unfilled CFASS tubes. Generally, the strength ratio increased almost linearly with both the D/t ratio and the concrete strength. Such variations are expected because a larger D/t ratio implies a larger concrete sectional area and a higher concrete strength implies a larger strength increase due to the infilling of concrete. On the other hand, the effect of ξ on the strength ratio is depicted by plotting the strength ratio against the value of ξ in Figure 16, from which it can be seen that as the value of ξ increased from 0.31 to 2.16, the strength ratio gradually decreased from the highest value of 4.80 to the lowest value of 1.61. This was because a larger D/t ratio and/or a higher concrete strength always lead to a lower ξ value but a higher strength ratio, causing the strength ratio to be inversely related to the ξ value.

4.3 Strain-hardening ductility performance

Whether the specimen had exhibited strain-hardening can be judged from the shape of its load-strain curve. If the load-strain curve, after passing through the point of 2% axial strain, gradually increased to reach an ultimate load (P_u) higher than the yield load (P_y), then it may be said that strain-hardening had occurred. The specimens that had exhibited strain-hardening are marked by "Yes" in the last column of Table 7. Out of the 26 concrete infilled CFASS tube specimens tested, 20 specimens had exhibited strain-hardening and the other 6 had not exhibited strain-hardening. Checking their ξ values, it is noted that those specimens that had exhibited strain-hardening had ξ values of 0.61 or higher, whereas those specimens that had not exhibited strain-hardening had ξ values of 0.50 or lower. Hence, as a rough guide, a minimum ξ value of 0.6 is needed for attaining strain-hardening ductility performance.

5. Assessment of codified design rules

There are still no design rules stipulated in any of the existing codes for the design of stainless steel circular tubes infilled with conventional concrete or SWSSC. Nevertheless, there are some design rules for the design of carbon steel circular tubes infilled with conventional concrete in the Eurocode EC4 [36], Australian Standard AS5100 [37], AISC Specification [38] and ACI Building Code ACI318 [39]. Whether these design rules could be applied also to stainless steel circular tubes infilled with conventional concrete or SWSSC is assessed in the following sub-sections.

5.1 Eurocode EC4 and Australian Standard AS5100:

The design equations provided in EC4 [36] and AS5100 [37] are the same. In Section 6.7.3 of EC4, the design equation for the nominal strength (P_{EC}) of CFST circular stub column under axial load is given as:

$$P_{EC} = f_{0.2} A_s \eta_{a0} + f_c A_c \left[1 + \eta_{c0} \frac{t}{D} \frac{f_{0.2}}{f_c}\right] \quad (1)$$

where the steel reduction factor η_{a0} and the concrete enhancement factor η_{c0} are to be determined using the following equations:

$$\eta_{a0} = 0.25\,(3 + 2\,\bar{\lambda}) \leq 1 \tag{2a}$$

$$\eta_{c0} = 4.9 - 18.5\,\bar{\lambda} + 17.0\,(\bar{\lambda})^2 \geq 0 \tag{2b}$$

In the above, $\bar{\lambda}$ is the relative member slenderness. A limit on the local slenderness of the steel tube is specified as $D/t\varepsilon^2 \leq 90$ in Table 6.3 of EC4. The same design equations as above are given in Section 10.6.2.2 of AS5100. However, the section slenderness limit is specified as $(D/t)(f_{0.2}/250) \leq 82$ in Section 10.2.3 and Table 10.2.4 of AS5100, which is somewhat different from that in EC4. In this study, the CFASS circular tubes used do not exceed the above slenderness limits in EC4 and AS5100. Hence, the EC4 and AS5100 would provide the same strength predictions.

5.2 AISC Specification

In AISC Specification [38], the design rules for the nominal strength (P_{AISC}) of CFST circular stub column under axial loading are stipulated in Section I2.2b. Steel circular sections in composite members subjected to axial loading are categorized as compact, non-compact or slender based on the D/t ratio. In this study, all the CFASS circular tubes used are compact sections based on the criterion $D/t \leq 0.15E_s/f_{0.2}$. Hence, the value of P_{AISC} may be determined by the following equation:

$$P_{AISC} = f_{0.2}A_s + 0.95\,f_cA_c \tag{3}$$

In the above equation, the strength enhancement due to the confinement effect of the steel tube on the concrete core has been neglected.

5.3 ACI Building Code ACI318

In ACI318 [39], the steel sections in composite members are not categorized into different types. Nevertheless, the steel circular sections should satisfy the condition $t \geq D[f_{0.2}/(8E_s)]^{0.5}$. In Section 22.4.2.2, the nominal strength (P_{ACI}) of CFST circular stub column under axial load is given by:

$$P_{ACI} = f_{0.2}A_s + 0.85\,f_cA_c \tag{4}$$

In the above equation, the strength enhancement due to the confinement effect of the steel tube on the concrete core has been neglected.

5.4 Comparisons of test yield loads with code predictions

The tested yield loads of the CFASS tubes infilled with SW-C35, SW-C70, SW-SS-C35 or SW-SS-C70 are compared with the respective predicted strengths by the various design codes in Table 8. In the calculations of the predicted strengths, all safety factors were set to unity, and the material properties obtained from the coupon tests (Table 1), the actual concrete strength at the time of testing day (Table 4) and the actual dimensions of the specimens (Table 6) were used.

In Table 8, the comparison is made in the form of tested yield load to prediction ratios. A ratio close to 1.0 indicates accurate prediction, whereas a ratio lower than 1.0 means un-conservative prediction and a ratio higher than 1.0 means conservative prediction. The mean and COV (coefficient of variation) of such ratios are presented in the last two rows of the table. Overall, since the mean P_y/P_{EC} ratio is equal to 0.96, which is lower than 1.0, the predictions by the EC4 and AS5100 are un-conservative. On the other hand, since the mean P_y/P_{AISC} ratio and the mean P_y/P_{ACI} ratio are equal to 1.28 and 1.36, which are both rather high, the predictions by the AISC and ACI are overly conservative. Relatively, the EC4 and AS5100 seem to provide more accurate and less scattered predictions compared to the AISC and ACI, as indicated by their mean P_y/P_{EC} ratio closer to 1.0 and relatively small COV.

Since the EC4 and AS5100 allow for the strength enhancement due to the composite action between the steel tube and the concrete core, but the AISC and ACI do not allow for such strength enhancement, it should be the strength enhancement that causes the difference between the strength predictions by these codes. To illustrate such difference, the tested yield load to prediction ratios of the various codes are plotted against the value of ξ in Figure 17. It is seen that the P_y/P_{EC} ratio varies only slightly with the value of ξ. On the other hand, the P_y/P_{AISC} and P_y/P_{ACI} ratios first increase with the value of ξ and then decrease when $\xi > 1.5$. Anyway, the P_y/P_{AISC} and P_y/P_{ACI} ratios vary quite widely and are consistently much too high. This is not satisfactory because the benefit of the significant strength enhancement has been wasted.

6. Assessment of design equation by Li *et al.*

Recently, the design method proposed by Han *et al.* [44] for carbon steel tubes infilled with conventional concrete was modified by Li *et al.* [15] and further refined by

Li *et al.* [33] for application to austenitic stainless steel tubes infilled with SWSSC. Their design equation was developed based on their own test results of Grade AISI 316 (EN 1.4401) austenitic stainless steel tubes infilled with SWSSC, as well as some other test results in the literature. The design equation so developed for the nominal strength (P_{Li}) is given by:

$$P_{Li} = (A_s + A_c)(1 + 1.41\,\xi)f_c \tag{5}$$

where the subscript of P_{Li} is the name of the first author of Ref.[33]. To evaluate the applicability of this equation, the tested yield loads are compared with the respective predicted strengths by this equation in the second last column of Table 8. As before, the comparison is made in the form of tested yield load to prediction ratios, and the mean and COV of such ratios are presented in the last two rows of the table. Overall, since the mean and COV of the P_y/P_{Li} ratios are equal to 0.91 and 0.061, respectively, this equation is un-conservative when applied to the specimens tested in this study.

To illustrate the variation of the prediction accuracy, the tested yield load to prediction ratios of this equation are plotted against the value of ξ in Figure 18. It is seen that the P_y/P_{Li} ratios vary quite widely and are consistently much too low. One possible cause is that Li *et al.* [33] used the proof load at 5% axial strain as the yield load when there was no peak within 5% axial strain, whereas in this study, the proof load at 2% axial strain was used instead. Frankly speaking, there is still no consensus on the value of axial strain to be adopted for determining the proof load. However, it is advocated herein that in a real column member, an axial strain of 2% is already quite large and an axial strain of 5% may not be reached during failure unless the other parts of the structure also have very good ductility. Hence, it should be more prudent to use the proof load at 2% axial strain in the structural design.

7. Proposed design equation

Herein, an attempt is made to develop a new and more accurate design equation for CFASS circular tubes infilled with different types of concrete, including SWSSC. First, the tested yield loads in this study are employed to develop a design equation for CFASS circular tubes infilled with SWSSC. Then, the test results for CFASS circular tubes infilled with other types of concrete obtained from the literature are employed to extend the design equation to different types of concrete.

From Figure 16, it appears that there is certain relation between the strength ratio (P_y/unfilled strength ratio) and the value of ξ. Although the unfilled strength, as listed in Table 5, is not exactly the same as $f_{0.2}A_s$ due to local buckling during testing, it is envisaged that there should be some correlation between the $P_y/(f_{0.2}A_s)$ ratio and the value of ξ. To investigate whether there could be any correlation, the $P_y/(f_{0.2}A_s)$ ratio of each specimen tested herein is plotted against the value of ξ in Figure 19. It is seen that the data points (marked by hollow squares) are very close to a curve, indicating that there is good correlation. To find out if such correlation also exists in the specimens tested by others, the test results of austenitic stainless steel (EN 1.4401) tubes infilled with SWSSC [15,32,33], austenitic stainless steel (EN 1.4301) tubes infilled with conventional concrete [41], stainless steel tubes infilled with conventional concrete [45], and austenitic stainless steel (EN 1.4301) tubes infilled with recycled aggregate concrete [46,47] have been analyzed. Details of these test specimens are presented in Table 9, where the specimen labels are same as the original ones in the literature. The $P_y/(f_{0.2}A_s)$ ratios of these specimens are also plotted in Figure 19. It is evident that all the data points, including those from this study and those from the literature, are very close to a curve, indicating that there is a sharp correlation.

It should be noted that dimensions of concrete cylinders were not mentioned in the Refs. [41,45,46], while the cylinder dimensions of 100 mm diameter × 200 mm height were used in Refs. [15,32,33]. The cylinder strengths of the concrete at columns testing day, or at the age of 28 days if the strengths at columns testing day not available, were used in the calculations in this study for a direct comparison between the design equations and the test results. For the specimens from Ref. [47], the 0.85 times the concrete cube strength was used to replace the cylinder strength in the calculation.

Regression analysis of the data presented Figure 19 has been carried out. The best-fit equation so derived is:

$$P_y/(f_{0.2}A_s) = 2.61\,\xi^{-0.46} \tag{6}$$

From this, the design equation for the nominal strength ($P_{C\&K}$) is obtained as:

$$P_{C\&K} = 2.61\,\xi^{-0.46}(f_{0.2}A_s) \tag{7}$$

In the above equation, the subscript of $P_{C\&K}$ is composed of the first letters of the names of the authors of this paper. To evaluate its applicability, the tested yield loads of the specimens tested herein are compared with the respective predicted strengths by this equation in the last column of Table 8 and the tested yield loads of the specimens tested by others are compared with the respective predicted strengths by this equation in the last column of Table 9. As before, the comparison is made in the form of tested yield load to prediction ratios, and the mean and COV of such ratios are presented in the last two rows of each table. For the specimens tested herein, the mean and COV of the $P_y/P_{C\&K}$ ratios are equal to 1.00 and 0.055, respectively, whereas for the specimens tested by others, the mean and COV of the $P_y/P_{C\&K}$ ratios are equal to 1.01 and 0.068, respectively. Hence, this equation is more accurate than the other existing equations and more importantly is widely applicable to different types of concrete infill, including SWSSC, conventional concrete and recycled aggregate concrete.

The $P_y/P_{C\&K}$ ratios of the specimens tested herein for CFASS tubes infilled with SWSSC and the specimens tested by others for CFASS tubes infilled with different types of concrete are all plotted against the value of ξ in Figure 20. That all the data points follow the same trend and fit very well into one single curve reveals that the use of SWSSC in place of conventional concrete as concrete infill in CFASS tubes has no significant effect on the yield strength of the infilled CFASS circular tubular stub columns.

8. Conclusions

The behaviour and design of cold-formed austenitic stainless steel (CFASS) circular tubular stub columns infilled with seawater sea-sand concrete (SWSSC) had been investigated. Totally, 31 CFASS circular tube specimens, 5 not infilled with any concrete and 26 infilled with concrete made with seawater and/or sea-sand, were tested under axial compression. The CFASS circular tubes had 5 different cross-sections with the diameter to thickness (D/t) ratios ranging from 20.4 to 53.6 whereas the SWSSC concrete mixes were of strength levels of 35 MPa and 70 MPa designed by replacing the fresh water with seawater and/or the fine aggregate with sea-sand. The findings from the experimental investigation are summarized below:

- The uses of seawater in place of fresh water and sea-sand in place of ordinary fine aggregate have little effects on the workability and strength of the concrete produced, and the axial behaviour of the infilled CFASS tubes. Hence, the use of SWSSC as concrete infill of stainless steel tubes is feasible, at least from the structural point of view.

- The axial load-strain curves and failure modes of the CFASS tubes infilled with SWSSC generally show the same features as those of the CFASS tubes infilled with conventional concrete of similar strength levels.
- CFASS tubes infilled with SWSSC also demonstrate the synergistic effects of increasing the yield load to higher than the sum of the strength of steel tube and the strength of concrete core, which may be quantified in terms of the strength enhancement index (*SEI*) defined by $SEI = P_y/(f_{0.2}A_s + f_cA_c)$. Within the ranges of parameters covered in this study, the *SEI* varies within 1.12 to 1.44.
- As for other concrete infilled steel tubes, the section constraining factor (ξ) defined by $\xi = f_{0.2}A_s/f_cA_c$ has major effects on the axial performance of the CFASS tubes infilled with SWSSC. Firstly, at $\xi > 0.6$, the CFASS tube infilled with concrete would exhibit strain-hardening ductility performance. Moreover, the *SEI* varies with ξ such that the *SEI* is highest when ξ is around 1.30.

The tested yield loads were used to assess the applicability of the existing design equations given in Eurocode EC4 [36], Australian Standard AS5100 [37], AISC Specification [38] and ACI Building Code ACI318 [39], as well as that proposed by Li *et al.* [33]. It was found that the design equations given in EC4 and AS5100 are un-conservative, whereas those given in AISC and ACI are overly conservative. The design equation by Li *et al.*, which incorporates the effects of ξ, is also un-conservative. To resolve this problem, a new design equation, which also incorporates the effects of ξ but in a different way, is proposed. It is developed based on the present test results of CFASS tubes infilled with SWSSC and the published test results of stainless steel tubes infilled with SWSSC, conventional concrete or recycled aggregate concrete. Very good agreement between the test results and the predictions by this new design equation has been achieved. Hence, the new design equation is widely applicable to stainless steel tubes infilled with different types of concrete. In fact, the feasibility of using just one design equation for stainless steel tubes infilled with different types of concrete, including SWSSC, is a good evidence that the use of SWSSC as concrete infill of stainless steel tubes has little effect on the yield load under axial compression.

Acknowledgments

The authors would like to thank the financial support from the Hong Kong Research Grants Council - Theme-based Research Scheme (Project No. T22-502/18-R), the assistance of Mr. C.Y. Chung, who helped to perform some of the tests as part of his final year undergraduate project, and the assistance of Ms. Vicky Fung, who measured the seawater chemical compositions.

References

[1] Y. Wei, C. Jiang, Y.-F. Wu. Confinement effectiveness of circular concrete-filled steel tubular columns under axial compression, J. Constr. Steel Res. 158 (2019) 15-27.

[2] J. Wei, X. Luo, Z. Lai, A.H. Varma. Experimental behavior and design of high-strength circular concrete-filled steel tube short columns, J. Struct. Eng. 146(1) (2020) 04019184.

[3] F.C. Wang, L.H. Han, W. Li. Analytical behavior of CFDST stub columns with external stainless steel tubes under axial compression. Thin-Walled Struct. 127 (2018) 756-768.

[4] F.C. Wang, L.H. Han. Analytical behavior of carbon steel-concrete-stainless steel double-skin tube (DST) used in submarine pipeline structure, Mar. Struct. 63 (2019) 99-116.

[5] S.P. Schneider. Axially loaded concrete-filled steel tubes, J. Struct. Eng. 124(10) (1998) 1125-1138.

[6] X.L. Zhao, L.H. Han, H. Lu. Concrete-Filled Tubular Members and Connections, Taylor & Francis, Oxford, UK (2010).

[7] D.K. Kim. A database for composite columns. MS thesis, School of Civil and Environmental Engineering, Georgia Institute of Technology, 2005.

[8] C.D. Goode. Composite columns-1819 tests on concrete-filled steel tube columns compared with Eurocode 4, Struct. Eng. 86(16) (2008) 33-38.

[9] L.H. Han, W. Li, R. Bjorhovde. Developments and advanced applications of concrete-filled steel tubular (CFST) structures: Members, J. Constr. Steel Res. 100 (2014) 211-228.

[10] J.F., Hajjar, B.C. Gourley, C. Tort, M.D. Denavit, P.H. Schiller, N. Leipziger Mundis. Steel-Concrete Composite Structural Systems, Department of Civil and Environmental Engineering, Northeastern University, Boston, Massachusetts, 2019, <http://www.northeastern.edu/compositesystems>.

[11] S. Thai, H.-T. Thai, B. Uy, T. Ngo. Concrete-filled steel tubular columns: Test database, design and calibration, J. Constr. Steel Res. 157 (2019) 161-181.

[12] J.-L. Ma, T.-M. Chan, B. Young. Material properties and residual stresses of cold-formed high strength steel hollow sections, J. Constr. Steel Res. 109 (2015) 152-165.

[13] M.X. Xiong, D.X. Xiong, J.Y.R. Liew. Axial performance of short concrete filled steel tubes with high- and ultra-high-strength materials, Eng. Struct. 136 (2017) 494-510.

[14] J. Xiao, C. Qiang, A. Nanni, K. Zhang. Use of sea-sand and seawater in concrete construction: Current status and future opportunities, Const. Build. Mater. 155 (2017) 1101-1111.

[15] Y.L. Li, X.L. Zhao, R.K. Raman Singh, S. Al-Saadi. Experimental study on seawater and sea sand concrete filled GFRP and stainless steel tubular stub columns, Thin-Walled Struct. 106 (2016) 390-406.

[16] N. Mahasenan, S. Smith, K. Humphreys. The Cement Industry and Global Climate Change: Current and Potential Future Cement Industry CO_2 Emissions. Proceedings of the 6th International Conference on Greenhouse Gas Control Technologies 1-4 October 2002, Kyoto, Japan. Volume II, 2003, pp995-1000.

[17] S.D. Ramaswamy, M.A. Aziz, C.K. Murthy. Sea dredged sand for concrete, extending aggregate resources, ASTM Int., 774 (1982) 167-177.

[18] S.K. Kaushik, S. Islam. Suitability of sea water for mixing structural concrete exposed to a marine environment. Cem. Concr. Compos. 17(3) (1995) 177-185.

[19] T.U.T. Mohammed, H. Hamada, T. Yamaji. Performance of seawater-mixed concrete in the tidal environment, Cem. Concr. Res. 34(4) (2004) 593-601.

[20] C.G. Girish, D. Tensing, K.L. Priya. Dredged offshore sand as a replacement for fine aggregate in concrete, Int. J. Eng. Sci. Emerg. Technol. 8(3) (2015) 88-95.

[21] Z. Dong, G. Wu, X.-L. Zhao, H. Zhu, J. Lian. Bond durability of steel-FRP composite bars embedded in seawater sea-sand concrete under constant bending and shearing stress, Const. Build. Mater. 192(20) (2018) 808-817.

[22] E.I. Diaz-Loya, E.N. Allouche, S. Vaidya. Mechanical properties of fly-ash-based geopolymer concrete, ACI Mater. J. 108 (2011) 300-306.

[23] G.S. Ryu, Y.B. Lee, K.T. Koh, Y.S. Chung. The mechanical properties of fly ash-based geopolymer concrete with alkaline activators, Const. Build. Mater. 47 (2013) 409-418.

[24] M. Chi. Mechanical strength and durability of alkali-activated fly ash/slag concrete, J. Marine Sci. Tech. 24(5) (2016) 958-967.

[25] M. Albitar, M.S. Mohamed Ali, P. Visintin, M. Drechsler. Durability evaluation of geopolymer and conventional concretes, Constr. Build. Mater. 136 (2017) 374-385.

[26] P. Nuaklong, V. Sata, P. Chindaprasirt. Properties of metakaolin-high calcium fly ash geopolymer concrete containing recycled aggregate from crushed concrete specimens, Constr. Build. Mater. 161 (2018) 365-373

[27] S. Tsivilis, E. Chaniotakis, G. Batis, C. Meletiou, V. Kasselouri, G. Kakali, A. Sakellariou, G. Pavlakis, C. Psimadas. Effect of clinker and limestone quality on the gas permeability, water absorption and pore structure of limestone cement concrete, Cem. Concr. Res. 21(2) (1999) 139-146.

[28] M. Sonebi, L. Svermova, P.J.M. Bartos. Factorial design of cement slurries containing limestone powder for self-consolidating slurry-infiltrated fiber concrete, ACI Mater. J. 101(2) (2004) 136-145.

[29] D.P. Bentz. Replacement of “coarse” cement particles by inert fillers in low W/C ratio concretes: II experimental validation, Cem. Concr. Res. 35(1) (2005) 185-188.

[30] M. Schneider, M. Romer, M. Tschudin, H. Bolio. Sustainable cement production - present and future, Cem. Concr. Res. 41(7) (2011) 642-650.

[31] L.G. Li, A.K.H. Kwan. Adding limestone fines as cementitious paste replacement to improve tensile strength, stiffness and durability of concrete, Cem. Conc. Compos. 60 (2015) 17-24.

[32] Y.L. Li, X.L. Zhao, R.K. Raman Singh, S. Al-Saadi. Tests on seawater and sea sand concrete-filled CFRP, BFRP and stainless steel tubular stub columns, Thin-Walled Struct. 108 (2016)163-184.

[33] Y.L. Li, X.L. Zhao, R.K. Singh Raman, X. Yu. Axial compression tests on seawater and sea sand concrete-filled double-skin stainless steel circular tubes, Eng. Struct. 176 (2018) 426-438.

[34] Z. Dong, G. Wu, X.-L. Zhao, H. Zhu, J.-L. Lian. Durability test on the flexural performance of seawater sea-sand concrete beams completely reinforced with FRP bars, Const. Build. Mater. 192 (2018) 671-682.

[35] Y.L. Li, X.L. Zhao, R.K. Singh Raman. Mechanical properties of seawater and sea sand concrete-filled FRP tubes in artificial seawater, Const. Build. Mater. 191 (2018) 977-993.

[36] EC4. Eurocode 4: Design of composite steel and concrete structures. 1-1: General rules and rules for buildings control, European Committee for Standardization (CEN) EN 1994-1-1, Brussels, Belgium: CEN, 2004.

[37] AS5100. Bridge design, part 6: steel and composite construction, AS 5100.6-2004, Standards Australia, Sydney, Australia, 2004.

[38] AISC. Specification for structural steel buildings, American Institute of Steel Construction, ANSI/AISC 360-16, Chicago, 2016.

[39] ACI. Building Code Requirements for Structural Concrete (ACI 318M-14) and Commentary (ACI 318RM-14), American Concrete Institute, Detroit, USA, 2014.

[40] Y. Cai, W.M. Quach, B. Young, Experimental and numerical investigation of concrete-filled hot-finished and cold-formed steel elliptical tubular stub columns, Thin-Walled Struct. 145 (2019) 106437.

[41] B. Uy, Z. Tao, L.H. Han. Behaviour of short and slender concrete-filled stainless steel tubular columns, J. Constr. Steel Res. 67(3) (2011) 360-378.

[42] M. Lai. Behaviour of CFST columns with external confinement under uni-axial compression, PhD Thesis (2015), The University of Hong Kong, Hong Kong.

[43] L. Li. Structural performance of concrete-filled cold-formed stainless steel members, PhD Thesis (2017), The University of Hong Kong, Hong Kong.

[44] L.-H. Han, G.-H. Yao, X.-L. Zhao. Tests and calculations for hollow structural steel (HSS) stub columns filled with self-consolidating concrete (SCC), J. Constr. Steel Res. 61 (2005) 1241-1269

[45] D. Lam, L. Gardner. Structural design of stainless steel concrete filled columns, J. Constr. Steel Res. 64(11) (2008) 1275-1282.

[46] V.W. Tam, Z.-B. Wang, Z. Tao. Behaviour of recycled aggregate concrete filled stainless steel stub columns, Mater. Struct. 47 (2014) 293-310.

[47] Y.-F. Yang, G.-L. Ma. Experimental behaviour of recycled aggregate concrete filled stainless steel tube stub columns and beams, Thin-Walled Struct. 66 (2013) 62-75.

Table 1: Material properties of the CFASS circular tubes.

$D \times t$ (mm×mm)	E_s (GPa)	$f_{0.01}$ (MPa)	$f_{0.2}$ (MPa)	f_u (MPa)	ε_u (%)	ε_f (%)	n
60.5×2.8	188.7	181.0	333.0	729.2	51.6	61.7	4.9
76.3×3.0	202.0	188.0	288.0	742.5	50.5	59.8	7.3
114.3×3.0	187.9	160.0	320.0	699.9	60.0	71.1	6.1
139.4×3.0	195.3	198.0	318.0	686.7	55.7	64.4	6.3
165.2×3.0	198.1	215.0	300.0	714.9	62.8	70.9	9.0

Table 2: Mix proportions of the concrete.

Concrete strength	Fine aggregate (kg/m^3)	10 mm aggregate (kg/m^3)	Cement (kg/m^3)	Water (kg/m^3)
C35	651.6	977.4	390.1	219.5
C70	651.6	977.4	538.4	171.8

Table 3: Chemical compositions of the seawater (%).

Na^+	Mg^{2+}	K^+	Ca^{2+}	Cl^-	SO_4^{2-}
1.04	0.14	0.06	0.05	2.55	0.24

Table 4: Workability and strength of the concrete.

Concrete label	Slump (mm)	28-day cylinder strength (MPa)			Cylinder strength at testing of CFST specimens (MPa)		
		1st test	2nd test	Average	1st test	2nd test	Average
C35	110	34.0	34.4	34.2	40.8	40.8	40.8*
C70	160	69.0	67.3	68.2	75.7	75.1	75.4*
SW-C35	110	33.2	34.2	33.7	39.2	38.7	39.0
SW-C70	190	72.8	73.0	72.9	80.6	73.4	77.0
SW-SS-C35	125	31.4	30.9	31.2	34.5	34.2	34.4
SW-SS-C70	225	75.1	74.8	75.0	73.9	74.0	74.0

Note: "*" means the cylinder strength was measured at the age of 60 days.

Table 5: Test results of the unfilled CFASS tubes.

Specimen label	D (mm)	t (mm)	L (mm)	A_s (mm^2)	P_{peak} (kN)	$P_{2\%}$ (kN)	P_u (kN)
60.5×2.8	60.50	2.91	150.7	527	-	197.6	262.3
76.3×3.0	76.35	3.11	190.0	716	-	251.7	323.2
114.3×3.0	114.38	3.07	285.0	1074	-	400.1	408.1
139.4×3.0	140.25	3.03	348.0	1306	-	459.2	459.3
165.2×3.0	165.10	3.10	412.0	1578	476.7	431.1	476.7

Table 6: Test results of the CFASS tubes infilled with concrete.

Specimen label	D (mm)	t (mm)	L (mm)	P_{peak} (kN)	$P_{2\%}$ (kN)	P_u (kN)
60.5×2.8-SW-C35	60.43	2.91	151.3	-	349.3	563.8*
60.5×2.8-SW-C35-r	60.53	2.89	151.0	-	351.2	581.2*
60.5×2.8-SW-C70	60.48	2.88	151.0	448.2	447.5	562.9*
60.5×2.8-SW-C70-r	60.48	2.96	151.0	440.0	439.0	543.4*
60.5×2.8-SW-SS-C35	60.55	2.89	151.0	-	326.7	460.6*
60.5×2.8-SW-SS-C35-r	60.38	2.89	151.0	-	317.4	462.6*
60.5×2.8-SW-SS-C70	60.50	2.89	151.0	429.0	428.6	470.0*
60.5×2.8-SW-SS-C70-r	60.40	2.92	151.0	456.0	454.1	487.1*
76.3×3.0-SW-C35	76.43	3.10	190.0	-	504.1	706.3*
76.3×3.0-SW-C35-r	76.33	3.10	190.0	-	512.5	636.3*
76.3×3.0-SW-C70	76.30	3.09	190.0	648.6	610.1	675.4*
76.3×3.0-SW-SS-C35	76.38	3.11	190.0	-	453.7	595.1*
76.3×3.0-SW-SS-C70	76.35	3.12	190.3	618.0	606.8	635.0*
114.3×3.0-SW-C35	114.40	3.08	285.0	-	877.0	945.4*
114.3×3.0-SW-C70	114.43	3.08	285.0	1184.3	1114.0	1184.3
114.3×3.0-SW-SS-C35	114.53	3.10	285.0	-	835.5	906.0*
114.3×3.0-SW-SS-C70	114.35	3.07	285.0	1245.0	1164.3	1245.0
139.4×3.0-SW-C35	140.08	3.04	348.0	-	1190.1	1191.1*
139.4×3.0-SW-C70	140.13	3.05	348.0	1789.4	1455.6	1789.4
139.4×3.0-SW-SS-C35	140.18	3.04	348.0	-	1098.2	1135.1*
139.4×3.0-SW-SS-C35-r	140.10	3.03	348.0	-	1110.6	1145.6*
139.4×3.0-SW-SS-C70	140.18	3.02	348.0	1711.3	1454.4	1711.3
165.2×3.0-SW-C35	164.98	3.09	412.0	-	1441.4	1442.7*
165.2×3.0-SW-C70	165.35	3.10	412.0	2290.5	1744.4	2290.5
165.2×3.0-SW-SS-C35	165.03	3.10	412.0	-	1315.8	1323.1*
165.2×3.0-SW-SS-C70	165.20	3.08	412.0	2269.0	1696.8	2269.0

Note: "*" means the ultimate load was only the maximum load recorded during the test.

Table 7: Analysis of the CFASS tubes infilled with concrete.

Specimen label	A_c (mm^2)	A_s (mm^2)	*SEI*	*D*/*t*	ξ	Strength ratio	Strain-hardening
60.5×2.8-SW-C35	2342	526	1.31	20.77	1.92	1.77	Yes
60.5×2.8-SW-C35-r	2354	523	1.32	20.94	1.90	1.78	Yes
60.5×2.8-SW-C70	2352	521	1.26	21.00	0.96	2.26	Yes
60.5×2.8-SW-C70-r	2338	535	1.23	20.43	0.99	2.22	Yes
60.5×2.8-SW-SS-C35	2356	524	1.28	20.95	2.15	1.65	Yes
60.5×2.8-SW-SS-C35-r	2341	522	1.25	20.89	2.16	1.61	Yes
60.5×2.8-SW-SS-C70	2352	523	1.23	20.93	1.00	2.17	Yes
60.5×2.8-SW-SS-C70-r	2338	527	1.30	20.68	1.01	2.30	Yes
76.3×3.0-SW-C35	3874	714	1.41	24.65	1.36	2.00	Yes
76.3×3.0-SW-C35-r	3863	713	1.44	24.62	1.36	2.04	Yes
76.3×3.0-SW-C70	3862	711	1.29	24.69	0.69	2.58	Yes
76.3×3.0-SW-SS-C35	3866	716	1.34	24.56	1.55	1.80	Yes
76.3×3.0-SW-SS-C70	3861	718	1.23	24.47	0.72	2.41	Yes
114.3×3.0-SW-C35	9202	1077	1.25	37.14	0.96	1.28	Yes
114.3×3.0-SW-C70	9207	1077	1.12	37.15	0.49	2.96	No
114.3×3.0-SW-SS-C35	9217	1085	1.26	36.95	1.10	2.09	Yes
114.3×3.0-SW-SS-C70	9197	1073	1.22	37.25	0.50	3.11	No
139.4×3.0-SW-C35	14103	1309	1.23	46.08	0.76	1.91	Yes
139.4×3.0-SW-C70	14109	1314	1.19	45.94	0.38	3.90	No
139.4×3.0-SW-SS-C35	14124	1310	1.22	46.11	0.86	2.39	Yes
139.4×3.0-SW-SS-C35-r	14111	1305	1.23	46.24	0.85	2.42	Yes
139.4×3.0-SW-SS-C70	14132	1301	1.17	46.42	0.40	3.73	No
165.2×3.0-SW-C35	19806	1572	1.16	53.39	0.61	2.50	Yes
165.2×3.0-SW-C70	19893	1580	1.14	53.34	0.31	4.80	No
165.2×3.0-SW-SS-C35	19813	1577	1.14	53.24	0.69	2.76	Yes
165.2×3.0-SW-SS-C70	19866	1569	1.17	53.64	0.32	4.76	No

Table 8: Comparison of tested yield loads to predictions by various design equations.

Specimen label	P_y/P_{EC}	P_y/P_{AISC}	P_y/P_{ACI}	P_y/P_{Li}	$P_y/P_{C\&K}$
60.5×2.8-SW-C35	0.93	1.33	1.38	0.84	1.03
60.5×2.8-SW-C35-r	0.94	1.34	1.39	0.85	1.04
60.5×2.8-SW-C70	0.98	1.30	1.37	0.86	0.97
60.5×2.8-SW-C70-r	0.95	1.26	1.33	0.83	0.94
60.5×2.8-SW-SS-C35	0.90	1.30	1.34	0.82	1.02
60.5×2.8-SW-SS-C35-r	0.88	1.27	1.31	0.80	1.00
60.5×2.8-SW-SS-C70	0.95	1.26	1.33	0.84	0.94
60.5×2.8-SW-SS-C70-r	1.01	1.34	1.41	0.88	1.00
76.3×3.0-SW-C35	1.03	1.44	1.51	0.96	1.08
76.3×3.0-SW-C35-r	1.05	1.47	1.54	0.98	1.10
76.3×3.0-SW-C70	1.03	1.33	1.42	0.93	1.02
76.3×3.0-SW-SS-C35	0.96	1.36	1.42	0.90	1.03
76.3×3.0-SW-SS-C70	0.99	1.29	1.37	0.90	0.99
114.3×3.0-SW-C35	0.94	1.28	1.35	0.93	0.96
114.3×3.0-SW-C70	0.93	1.16	1.25	0.89	0.94
114.3×3.0-SW-SS-C35	0.93	1.29	1.35	0.93	0.96
114.3×3.0-SW-SS-C70	1.00	1.26	1.35	0.96	1.01
139.4×3.0-SW-C35	0.95	1.27	1.35	0.96	0.96
139.4×3.0-SW-C70	1.01	1.23	1.33	0.98	1.06
139.4×3.0-SW-SS-C35	0.92	1.25	1.32	0.94	0.94
139.4×3.0-SW-SS-C35-r	0.94	1.27	1.34	0.95	0.95
139.4×3.0-SW-SS-C70	0.99	1.22	1.31	0.96	1.03
165.2×3.0-SW-C35	0.92	1.20	1.28	0.93	0.93
165.2×3.0-SW-C70	0.99	1.19	1.29	0.96	1.08
165.2×3.0-SW-SS-C35	0.89	1.17	1.25	0.90	0.90
165.2×3.0-SW-SS-C70	1.01	1.22	1.32	0.99	1.09
Mean	0.96	1.28	1.36	0.91	1.00
COV	0.048	0.058	0.049	0.061	0.055

Table 9: Assessment of proposed equation by comparing with test results in literature.

Data source	Specimen label	D (mm)	t (mm)	L (mm)	$f_{0.2}$ (MPa)	f_c (MPa)	P_y (kN)	$P_y/P_{C\&K}$
Li *et al.* [15]	S101-C	101.2	2.83	400	324.4	31.4	676	1.02
	S114-C	113.9	2.88	400	270.3	31.4	749	1.03
	S165-C	168.2	3.15	400	280.1	31.4	1449	1.04
Li *et al.* [32]	S50-C	50.9	3.07	150	228.2	35.8	205	0.99
	S101-C	101.9	2.79	400	225.7	35.8	555	0.95
	S114-C	114.1	2.79	400	280.7	35.8	745	0.96
	S165-C	168.4	3.22	400	281.1	35.8	1445	0.96
Li *et al.* [33]	50×1.6-F	49.6	1.53	150	376.5	42.0	202	0.97
	50×3-F	50.9	3.07	150	228.9	42.0	220	0.99
	76×1.6-F	76.2	1.66	230	398.9	42.0	372	0.87
	89×3-F	89.2	3.22	270	259.2	42.0	536	0.91
	101×1.6-F	101.8	1.70	300	353.3	42.0	612	0.97
	101×3-F	101.9	2.79	300	226.0	42.0	612	0.97
	114×3-F	114.1	2.79	350	281.2	42.0	831	0.99
	152×1.6-F	152.6	1.60	450	314.5	42.0	1050	1.00
	168×3-F	168.4	3.22	450	281.5	42.0	1635	1.01
	203×2-F	202.7	1.99	600	304.0	42.0	1787	1.02
Uy *et al.* [41]	C30-50×1.2A	50.8	1.20	150	291.0	30.0	151	1.05
	C30-50×1.6A	50.8	1.60	150	298.0	30.0	169	1.02
	C30-100×1.6A	101.6	1.60	300	320.0	30.0	494	1.00
	C30-127×1.6A	127.0	1.60	400	274.0	30.0	766	1.21
	C30-150×1.6A	152.4	1.60	450	279.0	30.0	937	1.12
	C30-200×2.0A	203.2	2.00	500	259.0	30.0	1537	1.11
Lam and Gardner [45]	CHS104×2-C30	104.0	2.00	300	412.0	31.0	679	1.02
	CHS104×2-C60	104.0	2.00	300	412.0	49.0	901	1.10
	CHS104×2-C100	104.0	2.00	300	412.0	65.0	1133	1.21
	CHS114×6-C30	114.3	6.02	300	266.0	31.0	1106	1.10
	CHS114×6-C60	114.3	6.02	300	266.0	49.0	1349	1.09
	CHS104×2-C100	114.3	6.02	300	266.0	65.0	1674	1.19
Tam *et al.* [46]	CS-0	168.9	2.86	510	339.6	41.2	1707	1.01
	CS-25	168.4	2.86	510	339.6	41.7	1595	0.94
	CS-50	169.7	2.86	510	339.6	41.0	1607	0.95
	CS-100	170.6	2.86	510	339.6	37.8	1573	0.96
Yang and Ma [47]	C-S-N	120.0	1.77	360	286.7	53.9#	823	1.00
	C-S-C1	120.0	1.77	360	286.7	50.7#	813	1.02
	C-S-C2	120.0	1.77	360	286.7	48.7#	802	1.02
	C-S-C3	120.0	1.77	360	286.7	48.4#	774	0.99
							Mean	1.01
							COV	0.068

Note: "#" means the value of f_c was calculated as 0.85 times the cube strength.

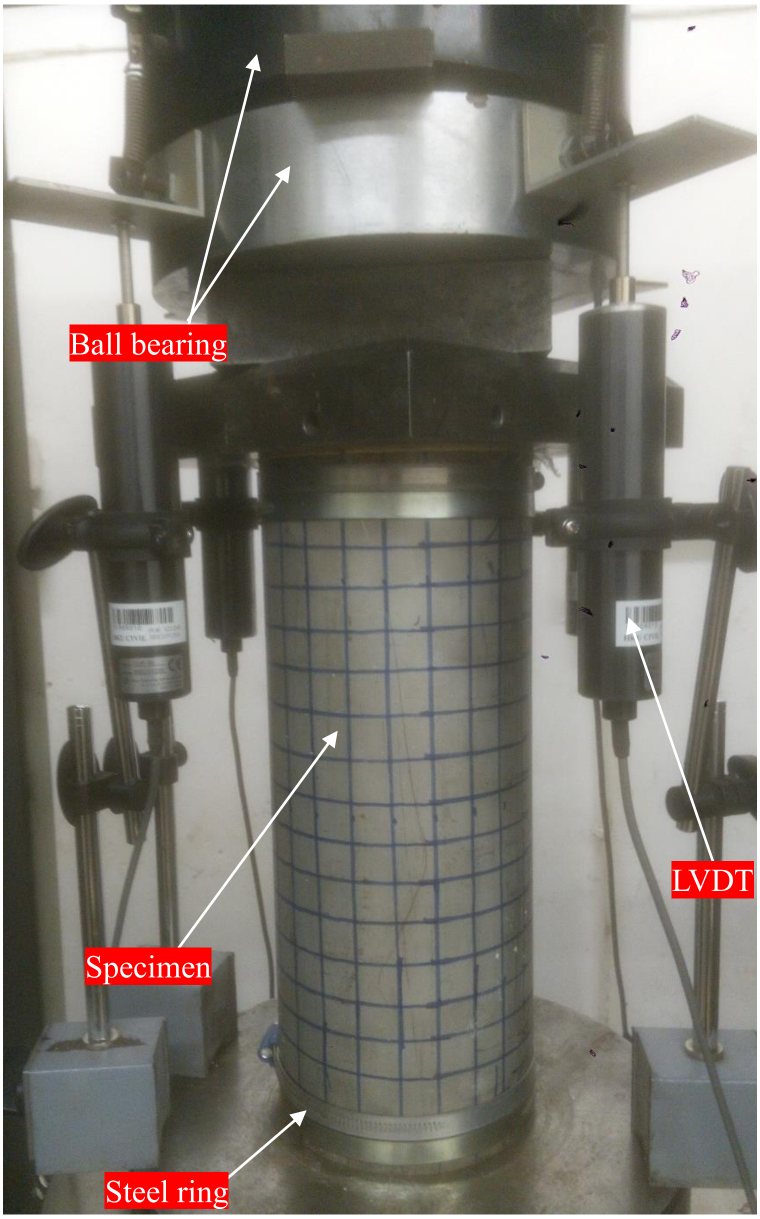

Figure 1: Test setup for specimen 165.2×3.0-SW-SS-C35.

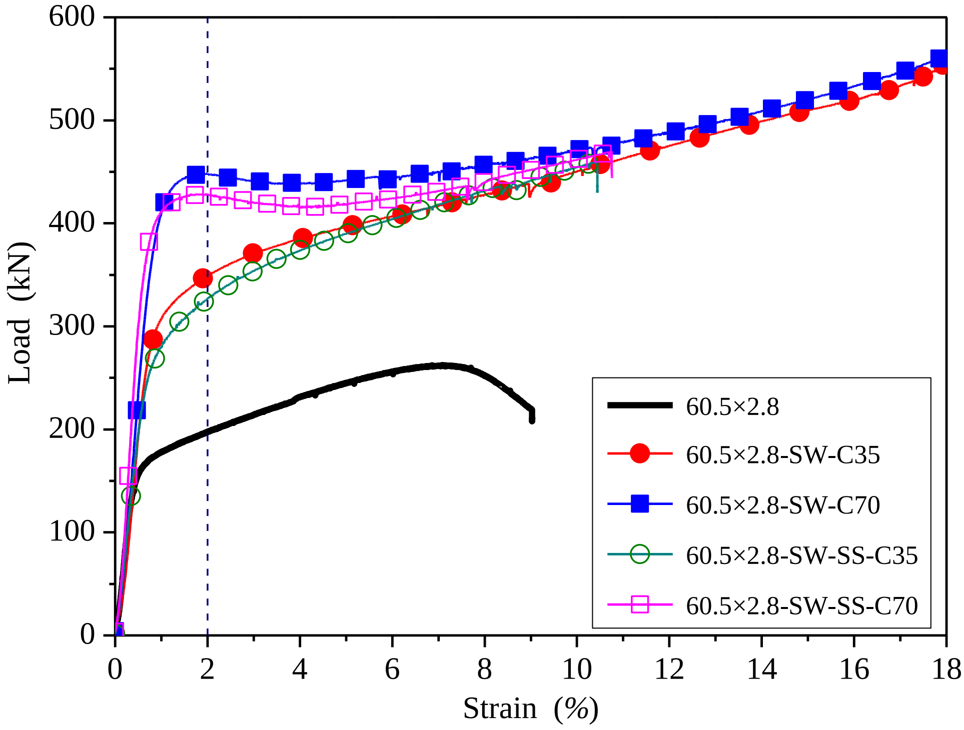

Figure 2: Load-strain curves of specimens with tube (D×t) size of 60.5×2.8.

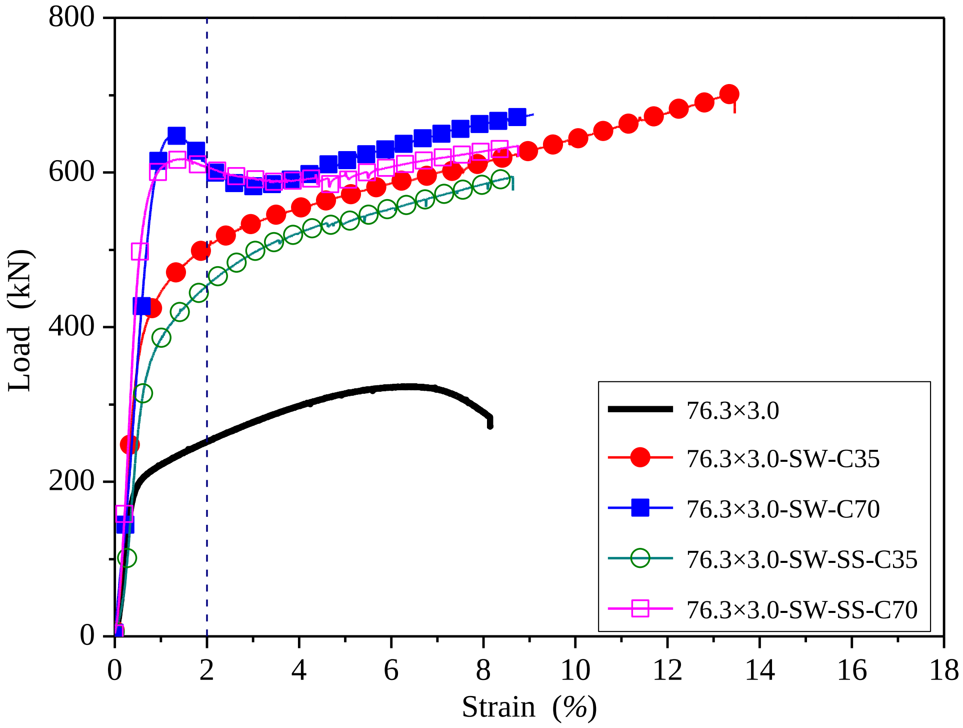

Figure 3: Load-strain curves of specimens with tube (D×t) size of 76.3×3.0.

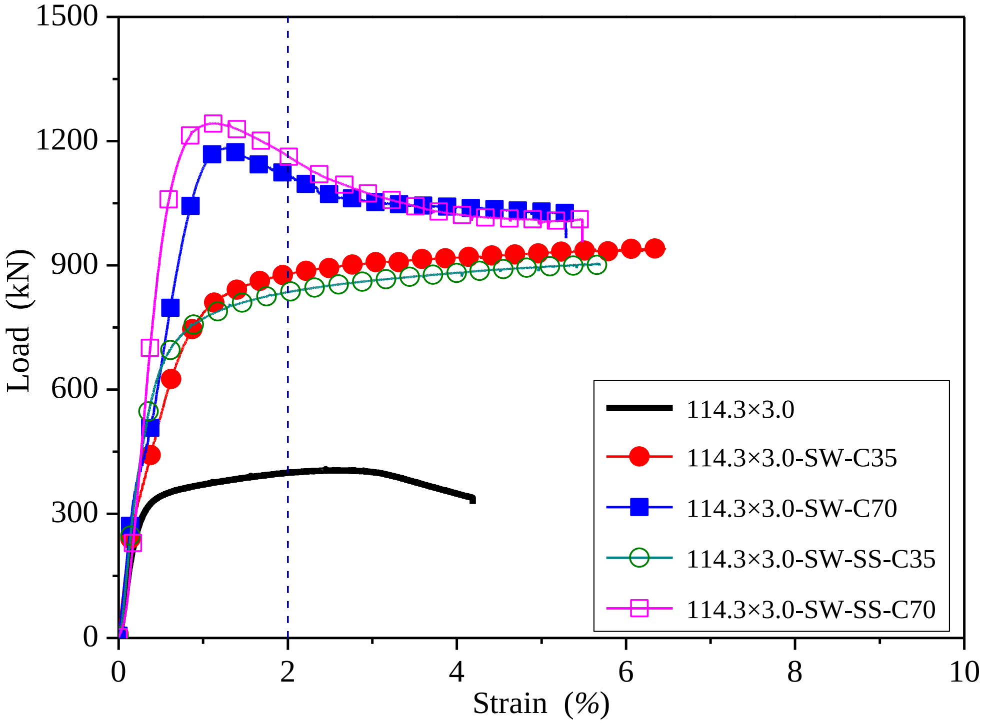

Figure 4: Load-strain curves of specimens with tube (D×t) size of 114.3×3.0.

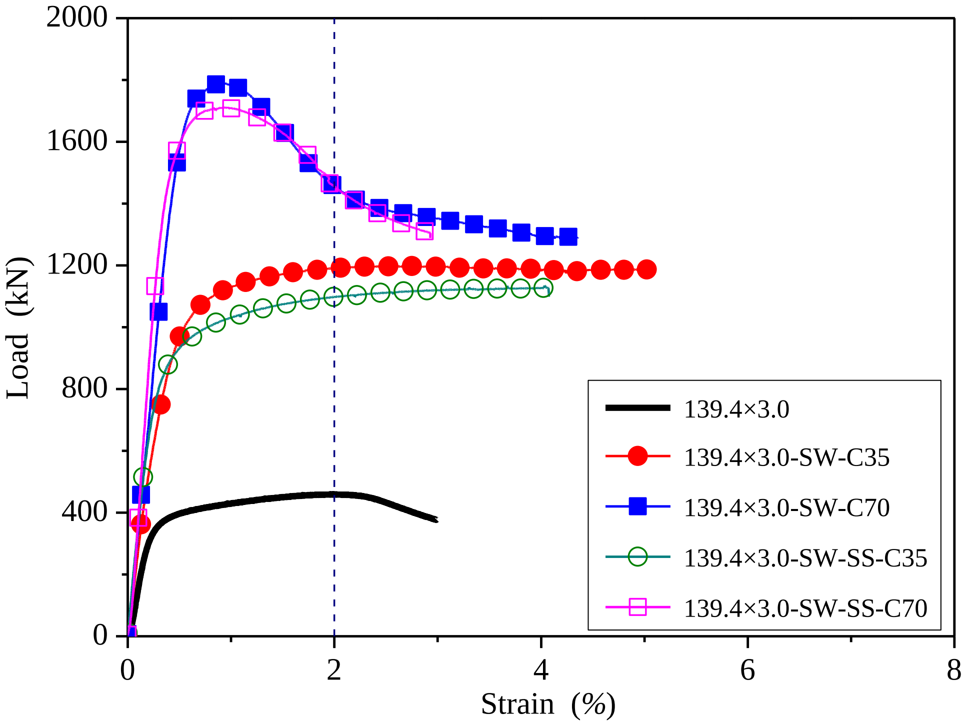

Figure 5: Load-strain curves of specimens with tube (D×t) size of 139.4×3.0.

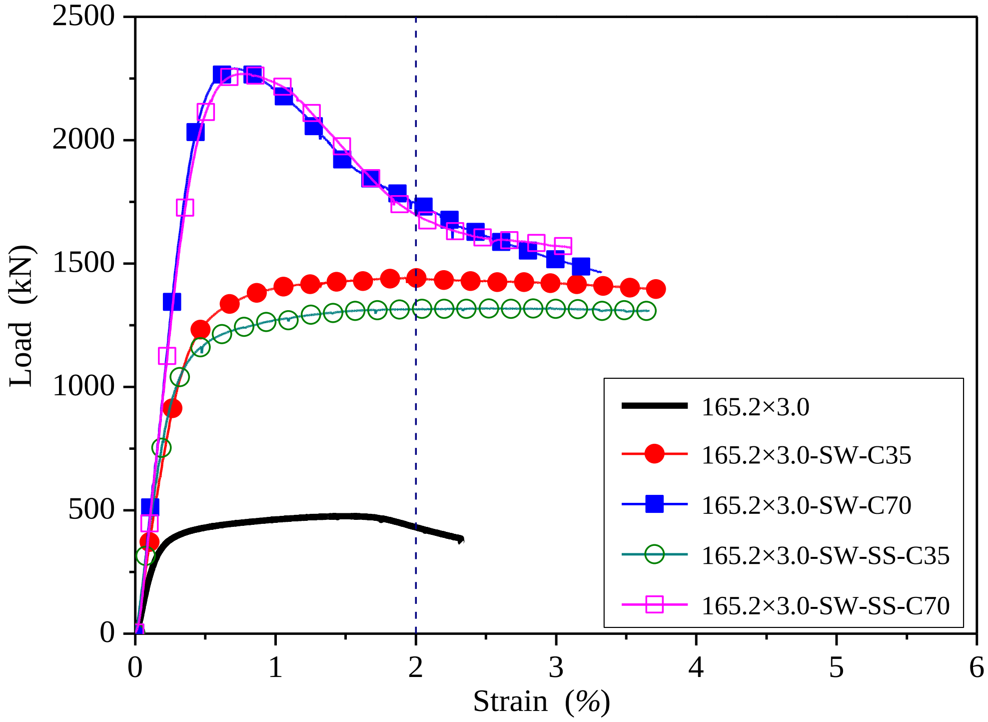

Figure 6: Load-strain curves of specimens with tube ($D \times t$) size of 165.2×3.0.

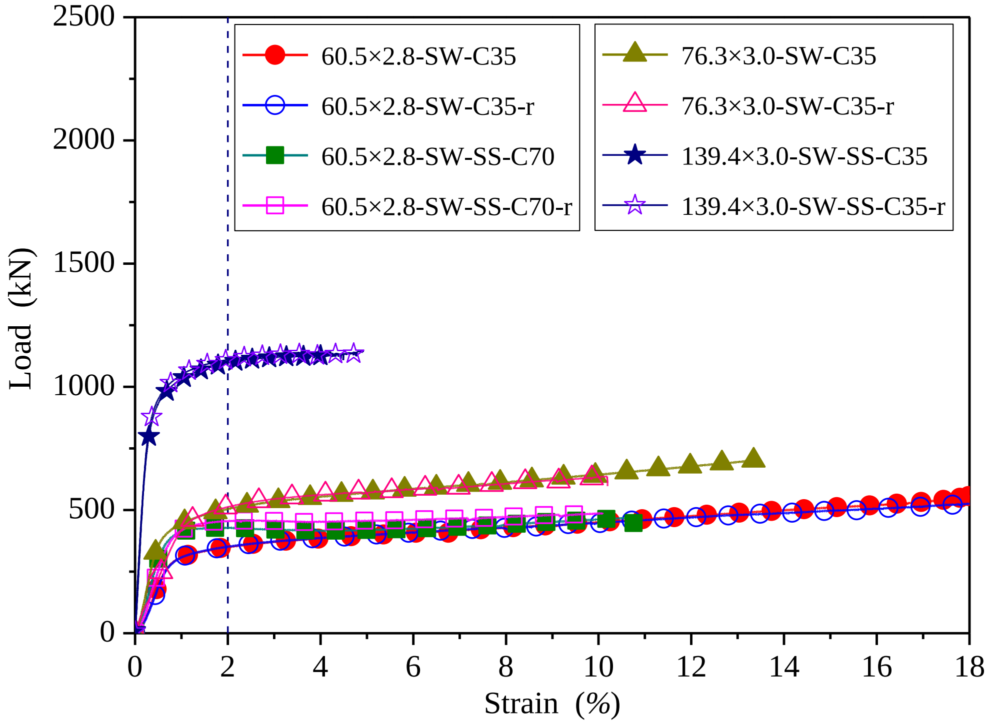

Figure 7: Comparison of load-strain curves of original and repeated specimens.

Figure 8: Failure modes of 60.5×2.8 (*left*) and 60.5×2.8-SW-C70 (*right*).

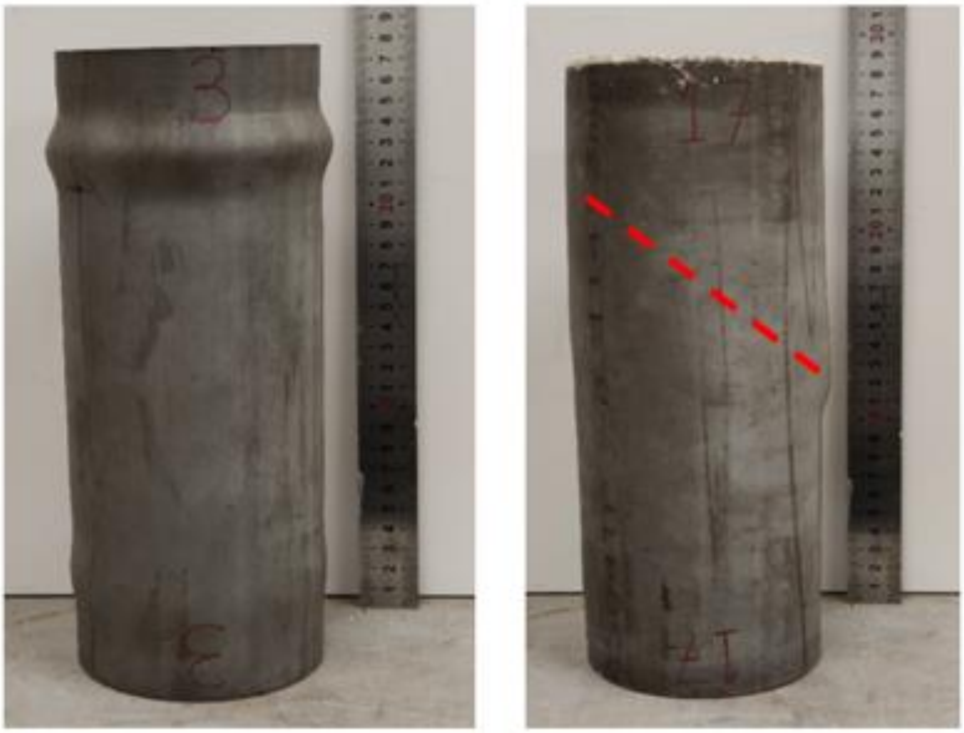

Figure 9: Failure modes of 114.3×3.0 (*left*) and 114.3×3.0-SW-C70 (*right*).

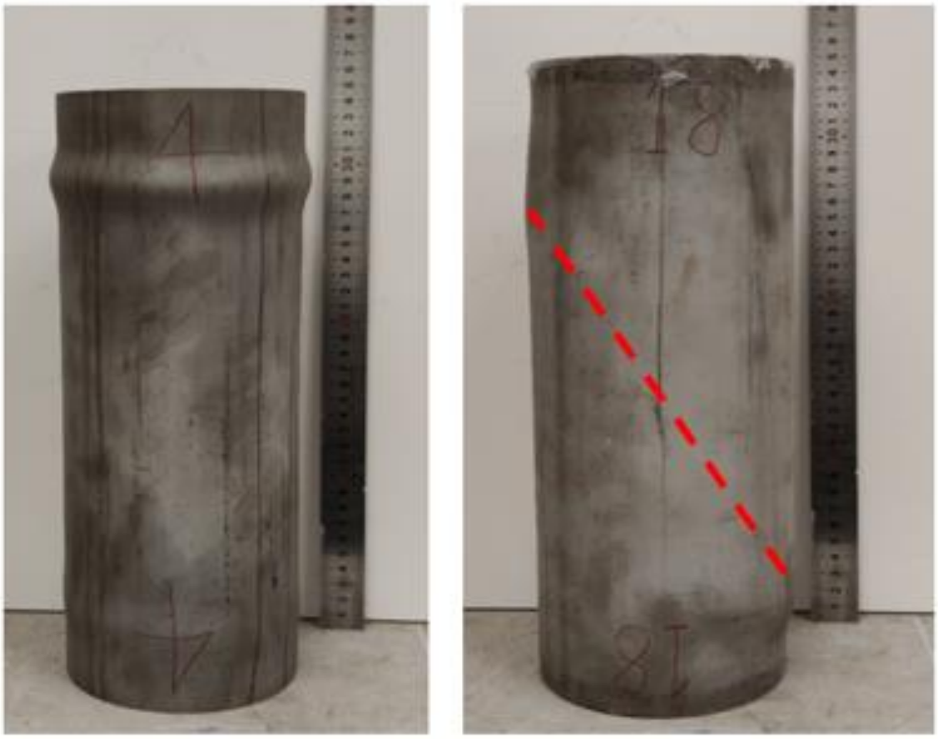

Figure 10: Failure modes of 139.4×3.0 (*left*) and 139.4×3.0-SW-C70 (*right*).

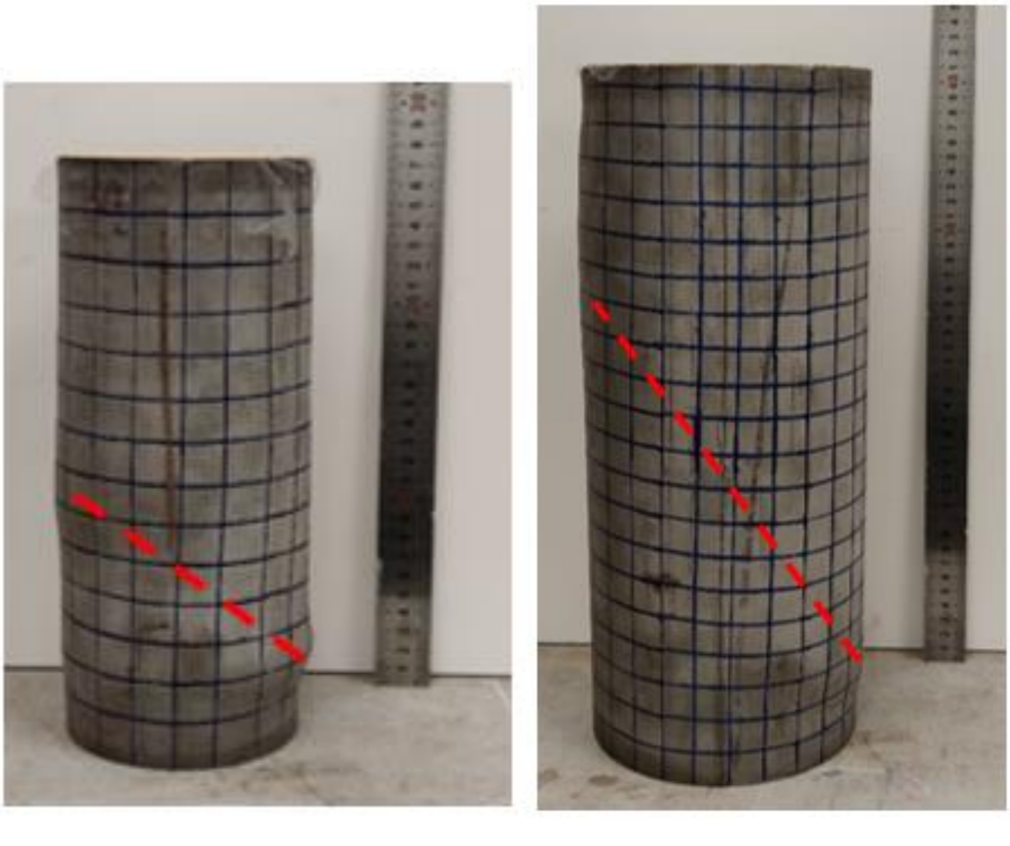

Figure 11: Failure modes of 114.3×3.0-SW-SS-C70 (*left*)
and 165.2×3.0-SW-SS-C70 (*right*).

Figure 12: Length and shape of 60.5×2.8-SW-C35
before testing (*left*) and after testing (*right*).

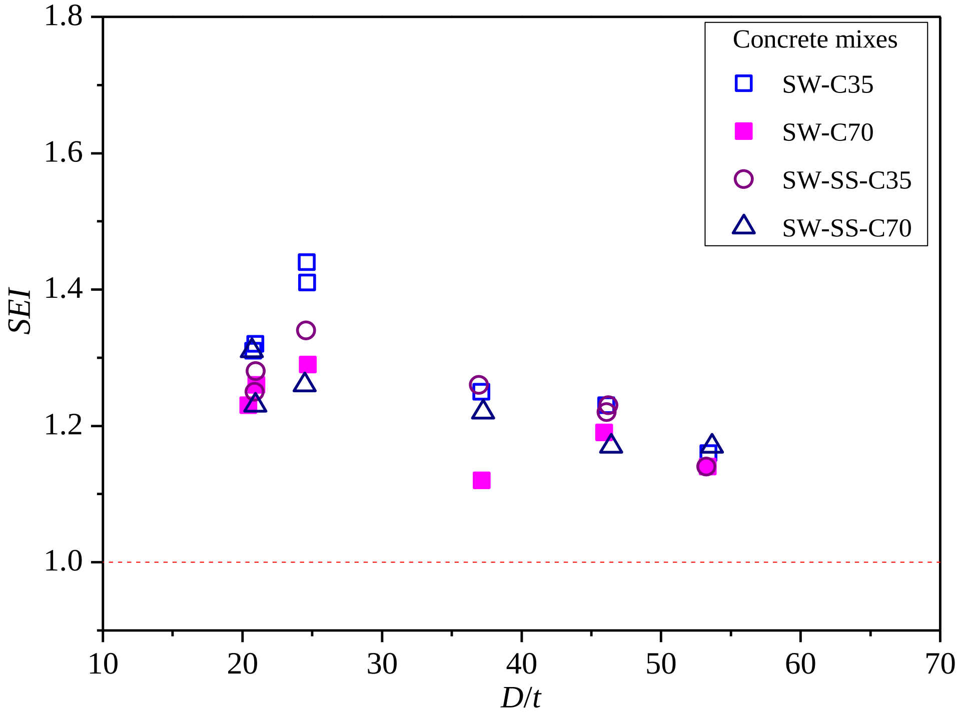

Figure 13: Variation of *SEI* with *D*/*t*.

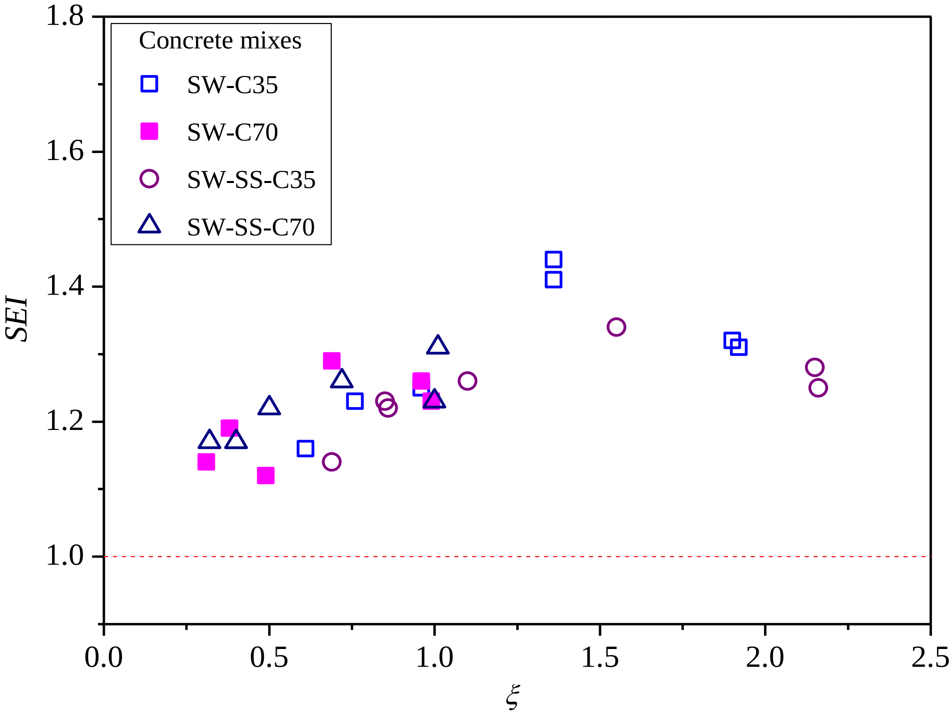

Figure 14: Variation of *SEI* with ξ.

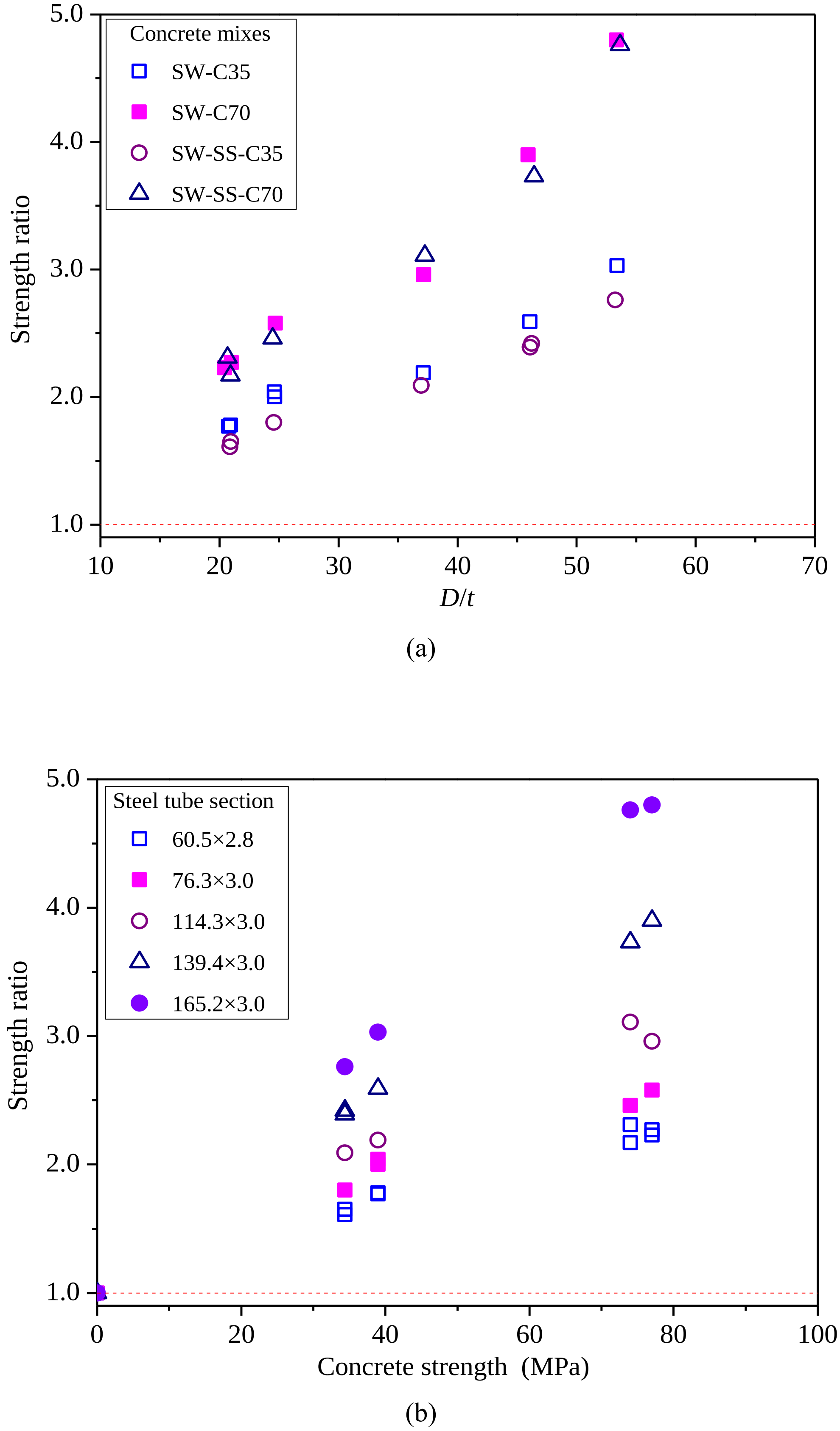

Figure 15: Variations of strength ratio with (a) D/t, and (b) concrete strength.

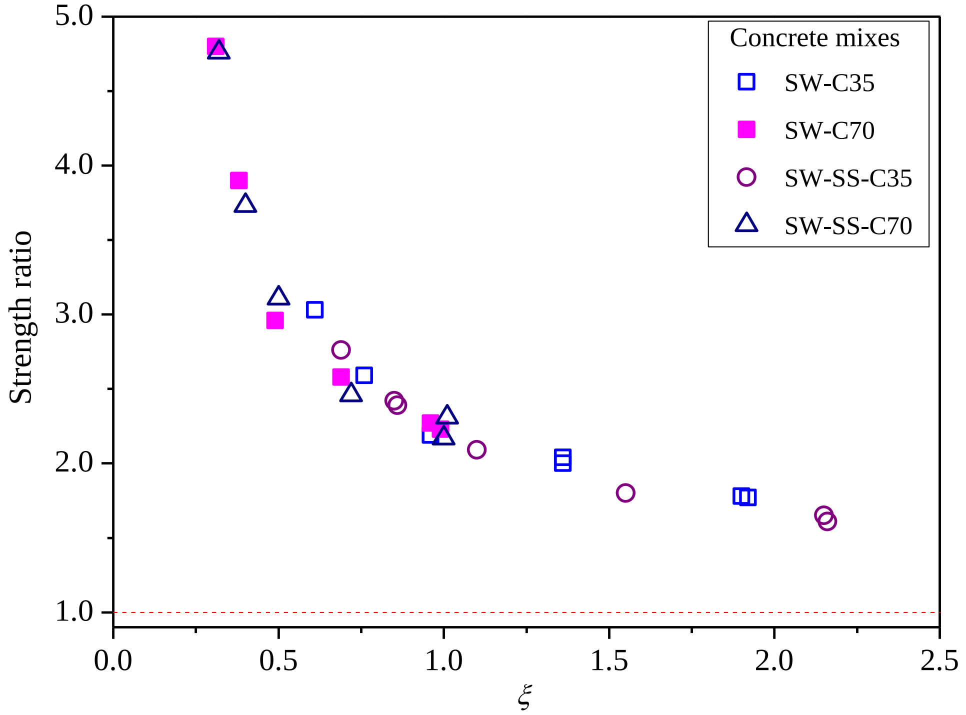

Figure 16: Variation of strength ratio with ξ.

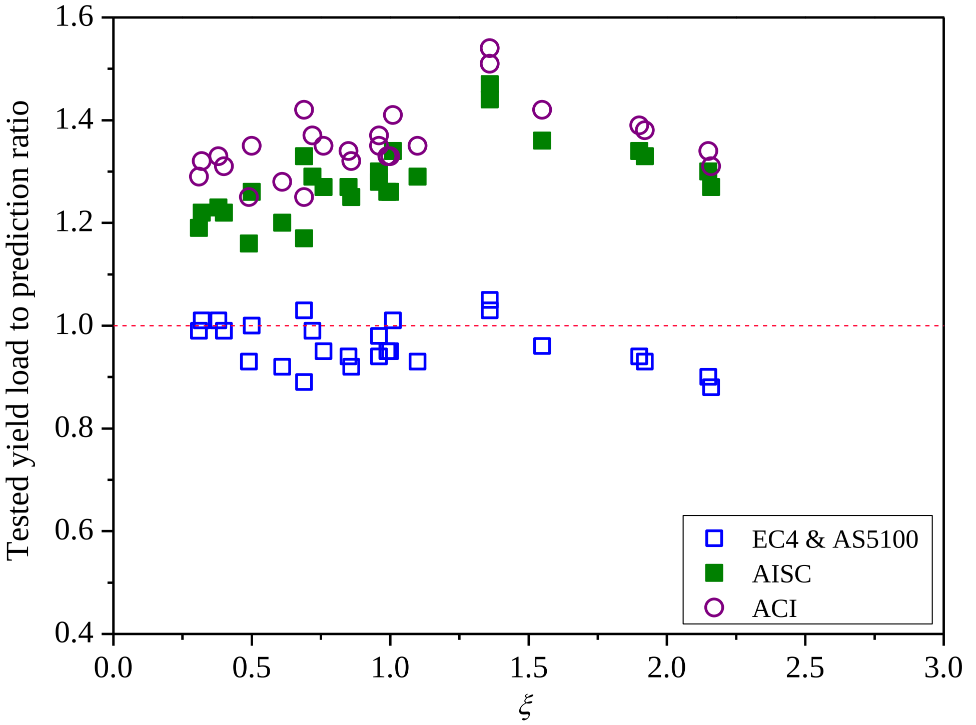

Figure 17: Comparison of test results with predictions by codes.

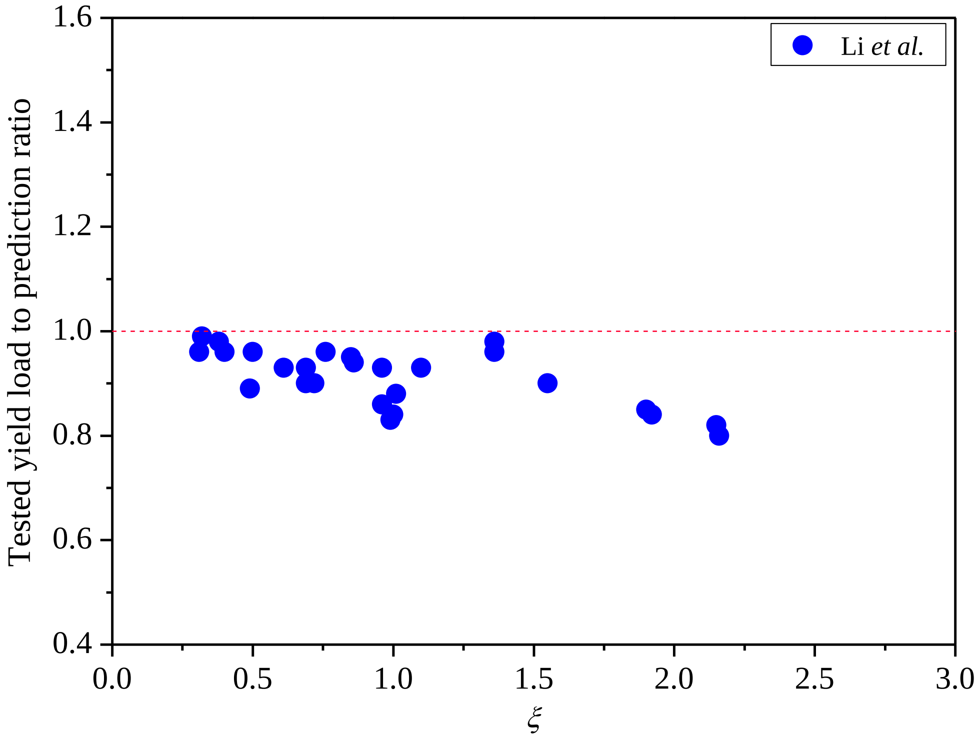

Figure 18: Comparison of test results with predictions by Li *et al*. [33].

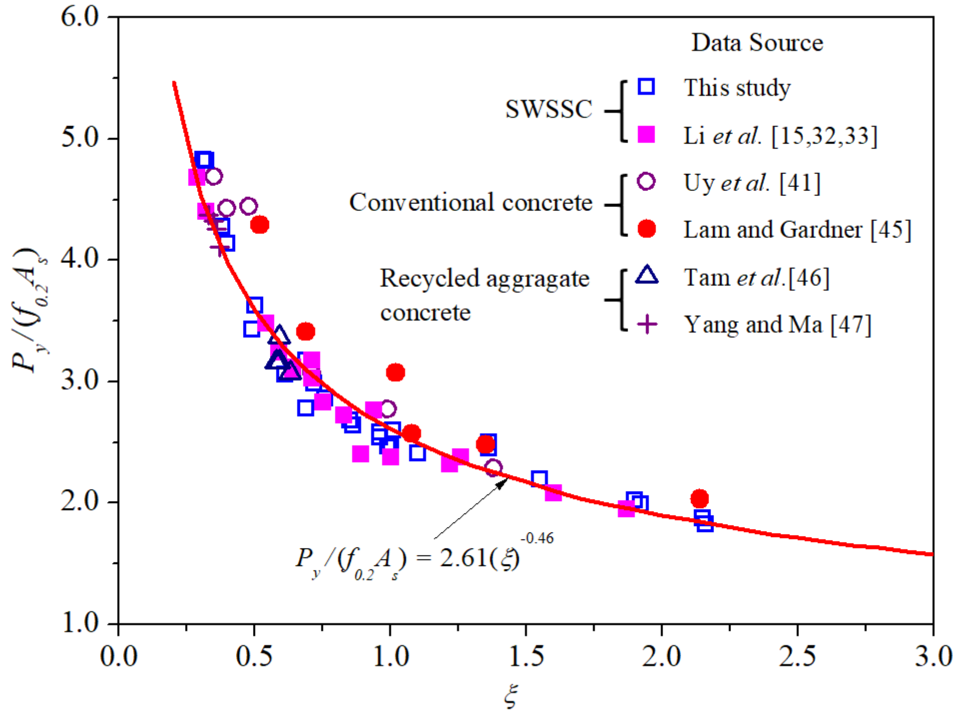

Figure 19: Relationship between $P_y/(f_{0.2}A_s)$ and ξ.

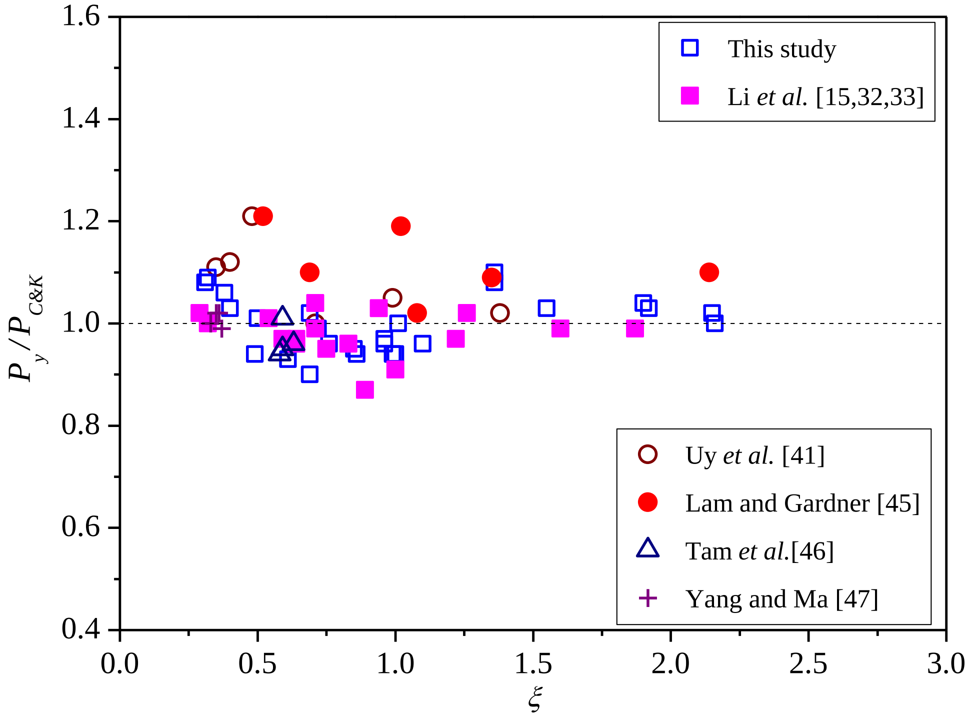

Figure 20: Comparison of test results from this study and literature with predictions by proposed equation.